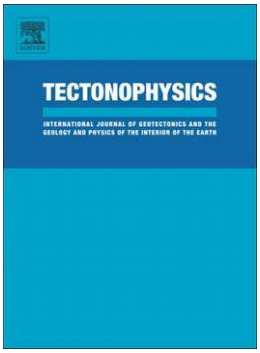

Refining seismic parameters in low seismicity areas by 3D trenching: the Alhama de Murcia fault, SE Iberia

Marta Ferrater, Maria Ortuño, Eulàlia Masana, Raimon Pallàs, Hector Perea, Stephane Baize, Eduardo García-Meléndez, José J. Martínez-Díaz, Anna Echeverria, Thomas K. Rockwell, Warren D. Sharp, Alicia Medialdea, Edward J. Rhodes

PII: S0040-1951(16)30136-6
DOI: doi: 10.1016/j.tecto.2016.05.020
Reference: TECTO 127107

To appear in: *Tectonophysics*

Received date: 18 November 2015
Revised date: 29 April 2016
Accepted date: 10 May 2016

Please cite this article as: Ferrater, Marta, Ortuño, Maria, Masana, Eulàlia, Pallàs, Raimon, Perea, Hector, Baize, Stephane, García-Meléndez, Eduardo, Martínez-Díaz, José J., Echeverria, Anna, Rockwell, Thomas K., Sharp, Warren D., Medialdea, Alicia, Rhodes, Edward J., Refining seismic parameters in low seismicity areas by 3D trenching: the Alhama de Murcia fault, SE Iberia, *Tectonophysics* (2016), doi: 10.1016/j.tecto.2016.05.020

Refining seismic parameters in low seismicity areas by 3D trenching: the Alhama de Murcia fault, SE Iberia

Marta Ferrater[1], Maria Ortuño[1], Eulàlia Masana[1], Raimon Pallàs[1], Hector Perea[2], Stephane Baize[3], Eduardo García-Meléndez[4], José J. Martínez-Díaz[5], Anna Echeverria[1], Thomas K. Rockwell[6], Warren D. Sharp[7], Alicia Medialdea[8], Edward J. Rhodes[8]

(1) RISKNAT Group. GEOMODELS. Departament de Geodinàmica i Geofísica, Facultat de Geologia, Universitat de Barcelona, c/ Martí i Franquès, s/n, 08028 Barcelona, Spain. Email: marta.ferrater@ub.edu

(2) Barcelona Center for Subsurface Imaging (B-CSI), Departament de Geociències Marines - Institut de Ciències del Mar - CSIC, 08003 Barcelona, Spain

(3) Institut de Radioprotection et Sûreté Nucléaire - Seismic Hazard Division (BERSSIN), BP 17, 92262 Fontenay-aux-Roses, France

(4) Área de Geodinámica Externa, Facultad de CC. Ambientales, Universidad de León, Campus de Vegazana s/n 24071 León, Spain

(5) Departamento de Geodinamica, Universidad Complutense, Instituto de Geociencias IGEO (UCM, CSIC), 28040 Madrid, Spain

(6) Department of Geological Sciences, San Diego State University, San Diego, CA 92182, USA

(7) Berkeley Geochronology Center, Berkeley, CA 94709, USA

(8) Landscape Dynamics, Department of Geography, University of Sheffield, Sheffield S10 2TN, UK

Three-dimensional paleoseismology in strike-slip faults with slip rates less than 1 millimeter per year involves a great methodological challenge. We adapted 3D trenching to track buried channels offset by the Alhama de Murcia seismogenic left-lateral strike-slip fault (SE Iberia). A fault net slip of 0.9 ± 0.1 mm/yr was determined using statistical analysis of piercing lines for one buried channel, whose age is constrained between 15.2 ± 1.1 ka and 21.9-22.3 cal BP. This value is larger and more accurate than the previously published slip rates for this fault. The minimum number of five paleo-earthquakes identified since the deposition of dated layers suggests a maximum average recurrence interval of approximately 5 ka. The combination of both seismic parameters yields a maximum slip per event between 5.3 and 6.3 m. We show that accurately planned trenching strategies and data processing may be key to obtaining robust paleoseismic parameters in low seismicity areas.

1. INTRODUCTION

Many regions undergoing rates of deformation below 5 millimeters per year are commonly perceived as seismically quiet even if a large historical earthquake has occurred. Hence, these regions are generally considered to be safe and to require low seismic protection standards. However, in such regions, elastic deformation may accumulate over long recurrence periods and be suddenly released in earthquakes that may be highly destructive, especially where the societal perception of hazard is limited (e.g. 2008 Mw7.9 Sichuan earthquake in China, Liu et al., 2016; 2003 Mw6.6 Bam earthquake in Iran, Wang et al., 2004). Paleoseismic studies were originally developed, and are most intensively applied, in active areas with high levels of seismicity. Few paleoseismic studies have focused on the characterization of the seismic potential of faults with slip rates under 5 mm/yr (Wesnousky et al., 1991; Lindvall & Rockwell, 1995; Marco et al., 2005). Applying paleoseismological methodologies to these tectonic settings, where erosion and sedimentation processes severely mask the effects of surface deformation, requires widening the time window and adapting widespread techniques originally developed in areas with high levels of seismicity (Ferrater et al., 2016).

The Alhama de Murcia fault (AMF; Fig. 1) belongs to the Eastern Betic Shear Zone (EBSZ), an active composite shear structure that absorbs part of the shortening between the Eurasian and African plates (4 – 6 mm/yr; Nocquet, 2012) in the SE Iberian Peninsula (De Larouziére et al., 1988). The AMF is a 87 km long left-lateral fault and has been subdivided into four sections (Silva, 1994; Martínez-Díaz, 1998; Martínez-Díaz et al., 2012a), the southernmost two showing the clearest evidence for late Quaternary activity (Goñar-Lorca and Lorca-Totana sections; Fig. 1C). The last significant earthquake caused by this seismogenic fault occurred in 2011 (Mw 5.2: López-Comino et al., 2012; Martínez-Díaz et al., 2012b), but paleoseismological information for the fault is scarce, incomplete, and involves large uncertainties (Silva et al., 1997; Martínez-Díaz et al., 2003; Masana et al., 2004; Ortuño et al., 2012).

Our study focuses on the 23 km long Lorca-Totana section of the AMF (Fig. 1C) where the 2011 earthquake occurred. The analysed section, with a N060E strike, in addition to a predominant strike-slip component, shows a vertical component of slip that lead to the uplift of La Tercia range (Martínez-Díaz, 1998; Ferrater et al., 2015), the source of extensive alluvial fans that drain towards the Neogene and Quaternary Guadalentín depression. Along this section, the fault splits into three major parallel strands: the north-dipping northern AMF (NAMF), the southern AMF (SAMF), that affects Pleistocene alluvial fans (Martínez-Díaz et al., 2003), and the frontal fault of the range (F-AMF); and minor sub-parallel traces (Fig. 1D). The NAMF is not amenable for a paleoseismic analysis because of the lack of late Quaternary sedimentation across the fault. Instead, paleoseismic studies along the

SAMF demonstrate its seismogenic behaviour and suggest the occurrence of a minimum of three paleoearthquakes in the past 27 kyr (Martínez-Díaz et al., 2003; Masana et al., 2004). In these studies, however, the slip rate for the SAMF in the Late Pleistocene has only been broadly constrained, and estimated to be between 0.07 and 0.66 mm/yr (Masana et al., 2004).

We carried out a three-dimensional paleoseismological analysis along the south strand (SAMF) of the AMF to demonstrate that this type of trenching program, together with numerical dating, and advanced statistical analyses, can be used to better determine directly and indirecly the seismic parameters of a seismogenic fault, even in slow tectonic settings. The aims of this paper are: a) to identify a long sequence of paleoearthquakes and calculate its recurrence period; b) to quantify the net dislocation of buried channels and obtain accurate mean slip rates; and c) to estimate a slip per event value and the maximum earthquake magnitude that is likely along the AMF. Our results improve the characterization of the seismic potential of the AMF and enhance the perception of its seismic hazard**.**

Approximate position of Figure 1

2. PALEOSEISMOLOGICAL SITE

At the El Saltador paleoseismological site, on the SAMF (Fig. 1D), the fault is vertical in deep creek outcrops and offsets the alluvial fans emanating from the La Tercia range. It uplifts the southeastern wall creating a smooth secondary NE-SW elongated ridge that blocks the southeastward-flowing drainages, an optimum context for paleoseismological studies (Fig. 1E). In the site area, the current creeks draining the fan surface do not show deflection at the fault crossing (Fig. 1E).

Ten new trenches were excavated at the El Saltador site (Fig. 2A): four were dug orthogonal to the fault trace to extend the paleoseismic catalogue, and six were excavated parallel to the fault to resolve the net slip rate of the SAMF. These parallel trenches were placed at a maximum distance of 40 m from the fault (TR12), and no closer than 2 m to it (TR14 and TR10) to avoid the zone of complex deformation within the fault zone. From a stratigraphic point of view, the trenches expose several alluvial units (J-X) and a system of channels entrenched on top of it (A-H; Fig. 2).

3. AGE CONTROL

To constrain the age of the units (A-X) exposed in the trenches, we used the radiocarbon technique on a snail and a charcoal sample, and Optically Stimulated Luminescence (OSL) dating of unit B, a fine-grained stratum (Table 1). The snail from unit G yielded a radiocarbon AMS age of 21,870 -

22,266 cal BP (2σ) and the charcoal sample from unit H (Fig. 2) an age of 25,883 - 25,279 cal BP (2σ; Table 1). The sample from unit B, analysed with OSL, yielded an age of 15.2 ± 1.1 ka (1σ; Table 1).

	Sample	Unit	Depth (m)	Moisture (%)	Dose rate (Gy/ka)	Equivalent dose (Gy)	Age (ka)
OSL Sample	SAL 27	B	0.87	5±2	2.67 ± 0.11	40.6 ± 2.3	15.2 ± 1.1
Radiocarbon sample	**Sample**	**Unit**	**Nature**	**Modern fraction**	**$D^{14}C$ (‰)**	**^{14}C age (BP)**	**Calibrated age BP**
	SAL 20	G	Snail	0.1036 ± 0.0006	-896.4 ± 0.6	18210 ± 45	21870-22266
	SAL 2	H	Charcoal			21210 ± 140	25228-25832

Table 1. Dating results of units B, G and H in the El Saltador paleoseismological site. Used techniques are Optically Stimulated Luminescence (OSL) for unit B and Radiocarbon (units G and H).

4. EVIDENCE OF PALEOEARTHQUAKES

The trenches at the El Saltador site exposed a sequence of deformed gravel and sand strata, interpreted as deposited in an alluvial fan environment, and a sequence of channelized units entrenched into the top of fan section. The alluvial sequence alternates with sand and silt layers with sparse matrix-supported clasts, interpreted as mudflow deposits (Fig. 2). The fault zone is composed mainly of a vertical fault and, north of it, a few faults displaying maximum dips of 45º to the south (Fig. 2; Masana et al., 2004), which together form a half flower structure. The secondary faults tend to increase their dip with depth (Masana et al., 2004) resulting in a fault zone that is locally more than five meters wide (Fig. 2, TR6). Faulting has locally generated fault-related folds, as that observed in trench 15, and has led to the formation of a progressive tectonic unconformity at the trench scale that is obvious in trenches 6 and 7 (Figs. 2C and 3).

The cumulated deformation is larger for the older exposed units, suggesting the occurrence of consecutive surface ruptures. The record of these ruptures is inferred using structural (tilting and fault displacement), stratigraphic (angular unconformities) and sedimentological (sudden changes in depositional environment caused by the obstruction of the drainage) criteria. Tracing the fault location was straightforward near the contact of different sedimentary units and particularly difficult through the silty layers. We will only describe here the five youngest ruptures recorded at this site (named events S1 to S5, from younger to older), which are the ones for which age-constraints are available. The event horizons are marked in Figure 2C. Event S1 produced the displacement of the base of unit A and underlying units, and is only traceable in trench 15, where it produced 12.5 cm of apparent vertical offset. Event S2 occurred after the deposition of unit B and prior to A, producing the fold exposed in trench 15, with an apparent vertical slip of 60 cm. The summed effect of events S1 and S2 is recorded

in trench 6 as a tilting of unit B, which dips ~12º towards the NW (against the natural slope of the fan, which drains towards the SE). Immediately below this tilted surface, we measured an 8 cm apparent dip displacement of the base of unit C along fault F4. Although it is not obvious, we cannot discard that this fault rupture propagates upwards through unit C. Because this unit is interpreted as a mudflow deposit (i.e. an instantaneous deposit), our preferred interpretation is to assume that F4 reaches the top of this layer. Placing the upward termination of the rupture at the base of C would imply that this rupture occurred simultaneously with the previous event recorded (event S3). Prior to event S2, solid evidence for a previous surface rupture (event S3) occurred between the deposition of unit C and D, as evidenced in trench 6 by the difference in tilt of their bases, which has led to an angular unconformity at the base of C. This relationship is also observed between units B and D at trench 7, although there, it is less straightforward. The record of this surface rupture is reinforced by the sedimentological and stratigraphic features of unit C, interpreted as a ponded stratum in the sense referred to by Rockwell et al. (2014); unit C is a matrix supported silt with sparse floating clasts, which possibly records a mudflow. It mantles the surface and thickens down flow towards the fault trace. Uplift caused by the SAMF during event S3 probably produced either a sufficiently large tectonic barrier or a counter-slope tilting of the surface that caused the ponding of mudflows near the fault. These relatively extensive mudflows deposits are not observed other than in a narrow corridor along the fault trace. Event S4 is identified in trench 6 by the angular unconformity between the base of unit D and underlying units, which are folded along fault F5. The oldest event analysed here, event S5, can be situated at the contact between units G and H. The existence of this event is based on three observations: 1) the base of unit G has a lower counter-slope dip than the base of H, obvious at trench 6 between faults F4 and F5; 2) at trench 6, the apparent vertical displacement of unit G along F5 (16 cm) is smaller than that of unit H (37 cm); and 3) unit G is interpreted as a mudflow deposit that ponded near the fault trace, in the same sense as explained above for unit C.

Two of the events described above have been correlated with the two events identified in trenches 3 and 4 in previous studies done by Martínez-Díaz et al. (2003) and Masana et al. (2004) in this area: event S2 corresponds to Event T and event S5 here would correspond to Event N.

According to these observations, the mean maximum earthquake recurrence interval is roughly estimated to be 5.0 – 5.2 ka considering that 5 events (S1 to S5) occurred after the deposition of unit H (25.8 – 25.2 kyr cal BP). If instead of five events, we consider just the two most recent ones (S1 and S2, both of which occurred since deposition of unit B), this recurrence interval becomes ~7.5 ka.

Approximate position of Figure 2

Approximate position of Figure 3

5. SLIP RATE

To estimate the net slip rate of the AMF, we followed the methodology proposed by Ferrater et al. (2016) valid for low sinuosity or short wavelength channels, i.e. those cases where a straight line may be adjusted to the channel shape. We used the present day channels on the surface of the El Saltador fan as an analogue for the shape of the past (buried) channels. The present-day channels (Fig. 1E) are not deflected by the fault and show very little sinuosity. Therefore, they can be simplified to a straight line.

Two possible channels may be recognized in unit D, although only the easternmost channel can be correlated univocally at both fault walls by its geometry and channel-fill facies with a low epistemic uncertainty (observed in trenches 14, 13, 10, and 5; Fig. 2D). To obtain the offset on this buried channel we identified reference points corresponding to the thalweg and to each of the channel margins in different trench walls and estimated the uncertainty on the position of each reference point. For the margins of the channel we used the top of unit D2 that is easy to differentiate from unit D1 in most of the trenches. Unit D1 presents tractive structures (laminar bedding and clast imbrication), whereas the lower part is erosive and has heterogenic and sub-angular blocks (Fig. 4 A and B). The uncertainties on the position of the reference points (taken with differential GPS) ranged between 2 m and 5 cm. In the southeastern wall, all channel features where surveyed in all trench walls (a total of four). However, in the northwestern wall, the margins were surveyed in four trench walls, and the thalweg in just two of them

We estimated a piercing line for each channel margin and for the thalweg by mathematically fitting the best straight line along the reference points (Fig. 4C; note that the best line might not cut into all the points as the fit is mathematical and the real line of the channel thalweg or margin might not be completely straight). The intersections of the piercing lines on both sides of the fault with the fault plane defined the 3D location of the piercing points. The distance between each pair of piercing points yielded a net offset value. The uncertainties in the piercing point locations on the fault plane were determined through a Monte-Carlo approach: we calculated hundreds of piercing points by projecting random possible straight lines that can be adjusted within the limits of the uncertainty ellipse of the reference point (Fig. 4C). The uncertainty of the piercing point is the standard deviation of all resulting

random piercing points. The mean offset values of the two margins and the thalweg and finally, the slip rate of the SAMF, were calculated using the Zechar and Frankel (2009) functions.

The dip of the fault plane can strongly influence the net offset results. Our model, following the field and trench observations, used a vertical fault plane (Fig. 2; Masana et al., 2004). In order to evaluate the influence of the dipping angle in the difference between the net and the vertical offset, we calculate the percentage difference for a few angles. For instance, for a fault dipping 80º, the net slip variation is 1%, and for a fault dipping 60º, the difference is 15%. We avoided the diffused deformation (among secondary faults) linked to the fault zone by taking reference points at a distance of a minimum of 2 m from the fault (trenches 10 and 14). The position of the modelled fault was set in the central part of the fault zone in order to calculate the contribution of the entire fault zone to the offset.

The result is a NNW-SSE oriented channel that cuts the fault at an oblique angle (Fig. 5). The mean net offset value for unit D (1σ) is $16.4\ ^{+2.7}/_{-0.3}$ m, with the strike slip component clearly predominant over the vertical one at a ratio of 12 to 1. The cumulated lateral displacement was caused by events S1, S2 and S3. The age of this channel is constrained between the ages of units B and G. Using the displacement probability distribution of the channel offsets and the age constraints (between 15.2 ± 1.1 ka and 21.9-22.3 cal BP), the best estimate for the net slip rate is 0.9 ± 0.1 mm/yr. Lateral and vertical slip rates are 0.9 ± 0.1 mm/yr and 0.1 ± 0.0 mm/yr, respectively.

Approximate position of Figure 4

Approximate position of Figure 5

6. DISCUSSION & CONCLUSIONS

3D trenching at El Saltador site provided, on one hand, the longest record of paleoearthquakes (5 seismic events) reported to date for the AMF, with a mean recurrence interval of ~5.1 ka for the past 25 ka. On the other hand, accurate analyses on channel offsets combined with numerical dating allowed the direct determination of the net slip rate of the SAMF, with a best estimate of 0.9 ± 0.1 mm/yr.

The newly calculated slip rate, restricted to the SAMF strand of the Lorca – Totana section of the AMF, is clearly larger than those considered to date for this fault section (Martínez-Díaz et al., 2003; Masana et al., 2004). The total net slip rate of the AMF must be even higher, considering that the contribution of the morphologically expressive NAMF and F-AMF (Figure 1) is not accounted for.

The SAMF fault strand shows a clear dominant lateral sense of slip (the obtained ratio between the lateral and the vertical component is 12:1). However, the orientation of the fault section with respect to the direction of convergence between the tectonic plates suggests that there should be a larger vertical component for the fault system. The probable vertical component of the NAMF is also suggested by 1) the uplift of the La Tercia range associated with the AMF activity (Ferrater et al., 2015; Fig. 1C), and 2) the oblique focal mechanism of the Mw 5.2 earthquake that occurred in the vicinity of Lorca in 2011 (Fig. 1C; López-Comino et al., 2012). This suggests that the NAMF and the F-AMF fault strands might absorb most of the vertical component of the deformation along this fault section.

We estimated the minimum slip per event by averaging the net offset by the total number of identified earthquakes. The calculated average of single event displacement since deposition of unit D is 5.3 – 6.3 m, considering an accumulated offset of 16.1 – 19.1 m produced by 3 events (a to c). As some seismic events may remain unrecognized in the paleoseismological record, the slip per event must generally be considered as a maximum value, which would also imply a considerably shorter recurrence interval if events are missing. Taking into account the very little sedimentation recorded for the past 15 ka (only unit A deposited during this period), it is plausible to consider the recurrence value, and thus the slip per event, as maximum values.

The maximum expected moment magnitude can be estimated from the empirical relationship determined by Anderson et al. (1996; $Mw = 5.12 + 1.16 \log L - 0.2 \log S$; where L is rupture length and S is net slip rate). The newly obtained slip rate (0.9 ± 0.1mm/yr) and the length of the AMF Lorca-Totana section (23 km) applied to this equation yield a moment magnitude of 6.7 ± 0.3. However, 5-6 m of lateral slip is large for this inferred magnitude and suggests that the AMF fault may rupture with adjacent fault sections in infrequent large earthquakes.

This study demonstrates that, even in slow tectonic settings, carefully selected paleoseismological sites may reveal long paleoearthquake records and allow estimation of key seismic parameters. A well-planned multi-trenching strategy may provide a sufficiently precise 3D reconstruction of depositional and deformational structures to support the application of rigorous statistical methods. This approach is crucial to achieve more robust results, especially in areas with neotectonic rates below 2 mm/a.

Acknowledgements

This research was funded by SHAKE CGL2011-30005-C02-02 and RISKNAT-2014SGR/1243. H. Perea was a fellow researcher under the "Juan de la Cierva" program. We thank José A. Álvarez Gómez and an anonymous reviewer for their comments improving the original manuscript.

REFERENCES:

Anderson, J.G., Wesnousky, S.G., and Stirling, M.W., 1996, Earthquake size as a function of fault slip rate: Bulletin of the Seismological Society of Americ, v. 86, no. 3, p. 683–690.

Liu, C., Zhu, B., Yang, X., and Shi, Y., 2016, Geodynamic background of the 2008 Wenchuan earthquake based on 3D visco-elastic numerical modelling: Physics of the Earth and Planetary Interiors, v. 252, p. 23–36.

Ferrater, M., Booth-Rea, G., Pérez-Peña, J.V., Azañón, J.M., and Masana, E., 2015, From extension to transpression: Quaternary reorganization of an extensional-related drainage network by the Alhama de Murcia strike-slip fault (eastern Betics): Tectonophysics, v. 663, p. 33-47. doi:10.1016/j.tecto.2015.06.011

Ferrater, M., Echeverría, A., Masana, E., Martínez-Díaz, J.J., and Sharp, W.D., 2016, A 3D measurement of the offset in paleoseismological studies: Computers & Geosciences, v. 90, p. 156-163.

De Larouziére, F.D., Bolze, J., Bordet, P., J., Hernández, J., Montenat, C., and Ott d'Estevou, P., 1988, The Betic segment of the lithospheric Trans-Alboran shear zone during the Late Miocene: Tectonophysics, v. 152, p. 41–52.

Lindvall, S.C., and Rockwell, T.K., 1995, Holocene activity of the Rose Canyon fault zone in San Diego, California: Journal of Geophysical Research, v. 100, p. 24121–24132.

López-Comino, J.Á., Mancilla, F.D.L., Morales, J., and Stich, D., 2012, Rupture directivity of the 2011, Mw 5.2 Lorca earthquake (Spain): Geophysical Research Letters, v. 39, no. 3, p. 1–5, doi: 10.1029/2011GL050498.

Marco, S., Rockwell, T.K., Heimann, A., Frieslander, U., and Agnon, A., 2005, Late Holocene activity of the Dead Sea Transform revealed in 3D palaeoseismic trenches on the Jordan Gorge segment: Earth and Planetary Science Letters v. 234, p. 189–205, doi: 10.1016/j.epsl.2005.01.017.

Martínez-Díaz, J.J., 1998, Neotectónica y Tectónica Activa del Sector Centro-Occidental de la Región de Murcia y Sur de Almería (Cordillera Bética – España) [Ph.D. thesis]: Madrid, Universidad Complutense de Madrid, 466 p.

Martínez-Díaz, J.J., Masana, E., Hernández-Enrile, J.L., and Santanach, P., 2003, Effects of repeated paleoearthquakes on the Alhama de Murcia Fault (Betic Cordillera , Spain) on the Quaternary evolution of an alluvial fan system: Annals of geophysics, v. 46, no. 5, p. 775–791.

Martínez-Díaz, J.J., Masana, E., and Ortuño, M., 2012a, Active tectonics of the Alhama de Murcia fault, Betic Cordillera, Spain: Journal of Iberian Geology, v. 38, no. 1, p. 253–270.

Martínez-Díaz, J.J., Bejar-Pizarro, M., Álvarez-Gómez, J.A., Mancilla, F.D.L., Stich, D., Herrera, G., and Morales, J., 2012b, Tectonic and seismic implications of an intersegment rupture The damaging May 11th 2011 Mw 5.2 Lorca, Spain, earthquake: Tectonophysics, v. 546-547, p. 28–37, doi: 10.1016/j.tecto.2012.04.010.

Masana, E., Martínez-Díaz, J.J., Hernández-enrile, J.L., and Santanach, P., 2004, The Alhama de Murcia fault (SE Spain), a seismogenic fault in a diffuse plate boundary: Seismotectonic implications for the Ibero-Magrebian region: Journal of Geophysical Research, v. 109, p. 1–17, doi: 10.1029/2002JB002359.

Nocquet, J.M., 2012, Present-day kinematics of the Mediterranean: A comprehensive overview of GPS results: Tectonophysics, v. 579, p. 220–242, doi: 10.1016/j.tecto.2012.03.037.

Ortuno, M., Masana, E., Garcia-Melendez, E., Martinez-Diaz, J., Stepancikova, P., Cunha, P.P., Sohbati, R., Canora, C., Buylaert, J.-P., and Murray, a. S., 2012, An exceptionally long paleoseismic record of a slow-moving fault: The Alhama de Murcia fault (Eastern Betic shear zone, Spain): Geological Society of America Bulletin, v. 124, no. 9-10, p. 1474–1494, doi: 10.1130/B30558.1.

Rockwell, T.K., Ragona, D.E., Meigs, A.J., Owen, L. a., Costa, C.H., and Ahumada, E. A., 2014, Inferring a thrust-related earthquake history from secondary faulting: A long rupture record of La Laja fault, San Juan, Argentina: Bulletin of the Seismological Society of America, v. 104, no. 1, p. 269–284, doi: 10.1785/0120110080.

Silva, P.G., 1994, Evolución Geodinámica de la Depresión del Guadalentín desde el Mioceno superior hasta la Actualidad: Neotectónica y Geomorfología [Ph.D. thesis]: Madrid, Universidad Complutense de Madrid, 642 p.

Silva, P.G., Goy, J.L., Zazo, C., Lario, J., and Bargají, T., 1997, Paleoseismic indications along “aseismic”fault segments in the Guadalentín depression (SE Spain): Journal of Geodynamics, v. 24, no. 1-4, p. 105–115.

Wang, R., Xia, Y., Grosser, H., Wetzel, H.-U., Kaufmann, H., and Zschau, J., 2004, The 2003 Bam (SE Iran) earthquake: precise source parameters from satellite radar interferometry: Geophysical. Journal International, v. 159, p. 917–922

Wesnousky, S.G., Prentice, C.S., and Sieh, K.E., 1991, An offset Holocene stream channel and the slip rate along the northern reach of the San Jacinto fault zone, San Bernardino Valley, California: Geological Society of America Bulletin, v. 103, p. 700–709.

Zechar, J.D., and Frankel, K.L., 2009, Incorporating and reporting uncertainties in fault slip rates: Journal of Geophysical Research, v. 114, no. B12, p. B12407, doi: 10.1029/2009JB006325.

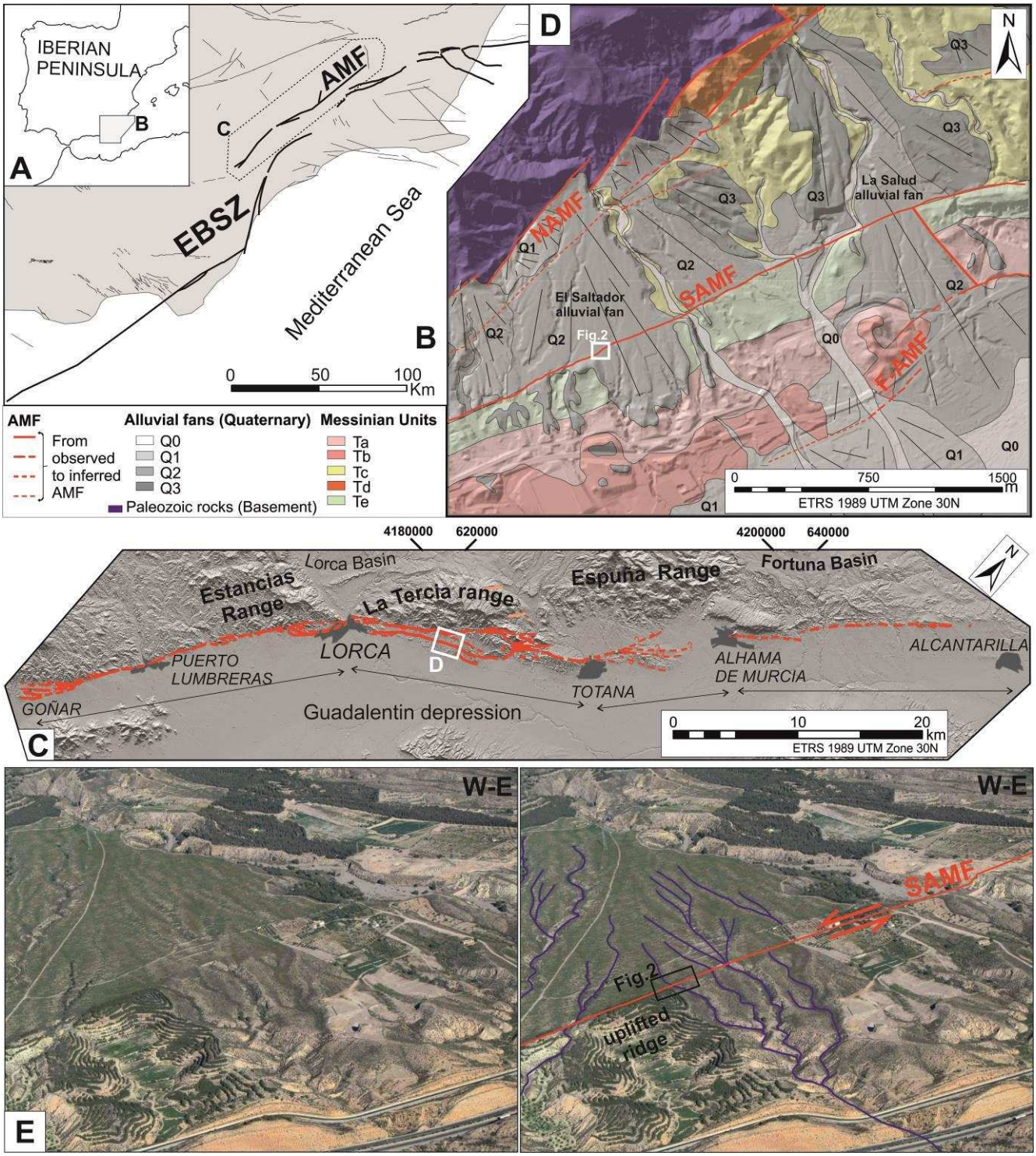

Figure 1. A and B) Location of the study area in the Eastern Betics Shear Zone (EBSZ faults in bold line); C) structural map of the AMF, where fault sections are highlighted; D) geological map of El Saltador alluvial fan where the white square indicates the El Saltador trenching site (legend: Ta-e, Upper-Messinian rocks; $Q_{0\text{-}3}$, Quaternary alluvial phases from older (3) to younger (0)); E) oblique

aerial view of the El Saltador alluvial fan surface towards the north; the streams maintain their orientation while crossing the fault.

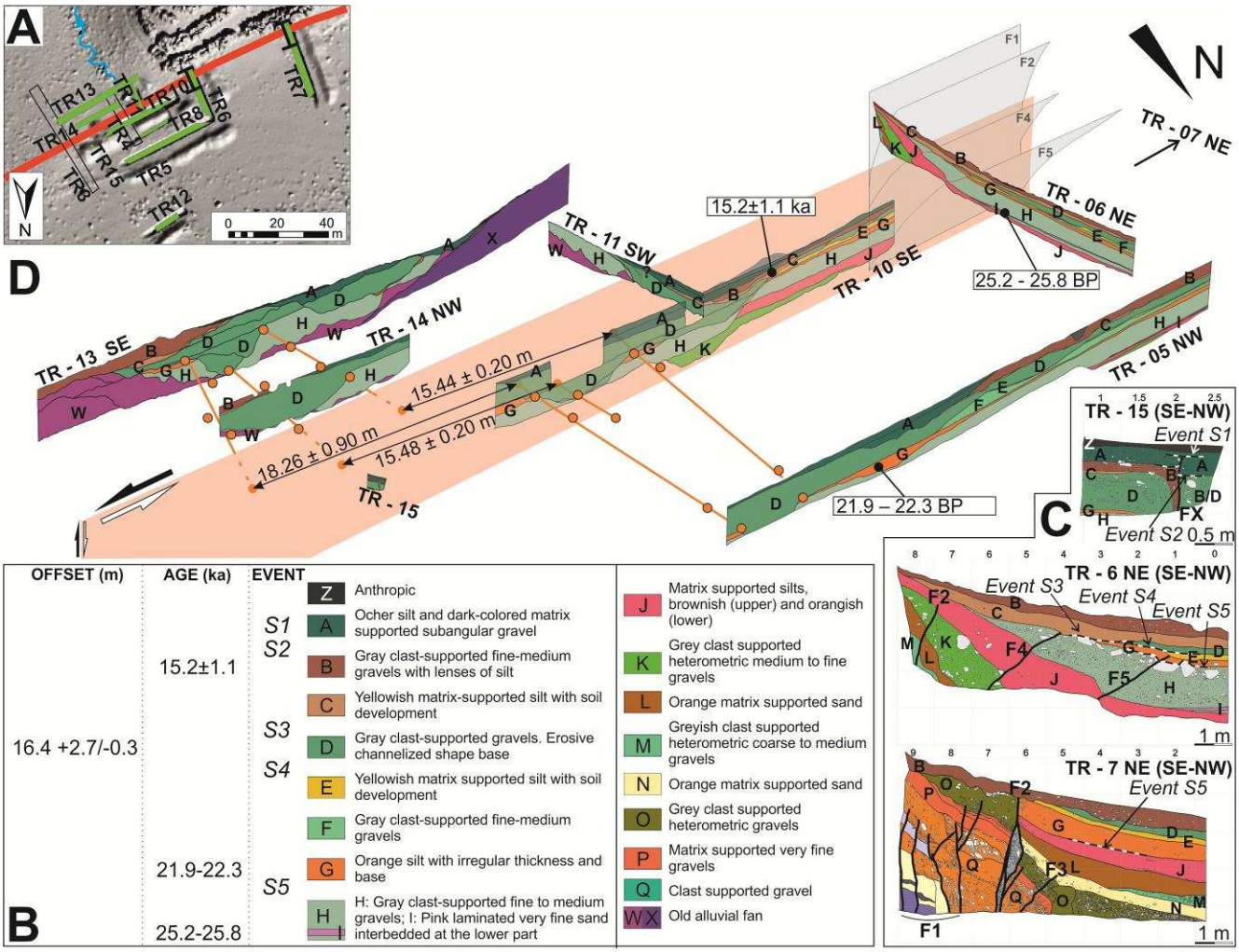

Figure 2. Results at El Saltador site. **A**) Map with the trench locations of this study in green (the position of the trenches 3 and 4 in Masana et al., 2004 is highlighted), the fault zone in red, and the position of the active channel (blue). **B**) Legend summarizing units' description, offset measurements, numerical ages and identified events. **C**) Partial logs of the trenches dug across the fault showing deformed stratigraphic units (TR 6, 7 and 15, position indicated in 2A and D) with indication of the event horizons (dashed black and white lines, S1 to S5). Interpretation of events is based on: event S1: unit A is offset while unit Z shows no deformation (Trench 15); event S2: unit B is more strongly folded than unit A (Trench 15); event S3: angular discontinuity between units D and C (Trench 6); event S4: unit D is not affected by the deformation that folds unit G and E (Trench 6); events S5: the base of unit H dips more that the base of unit G (Trench 6); **D**) Perspective block diagram showing the location of some trench walls (TR 5 NW, 6 NE, 10 SE, 11 SW, 13 SE, 14 NW and 15; the others are

not included for clarity), the reconstructed fault plane and the samples position. Orange dots on channels in the trench walls represent the position of all reference points. In orange, piercing lines and piercing points for channel D. The piercing lines have been adjusted using two to four reference points for each channel feature (rims or thalweg). Piercing lines are regression lines and thus do not necessarily contain the reference points due to channel irregularities.

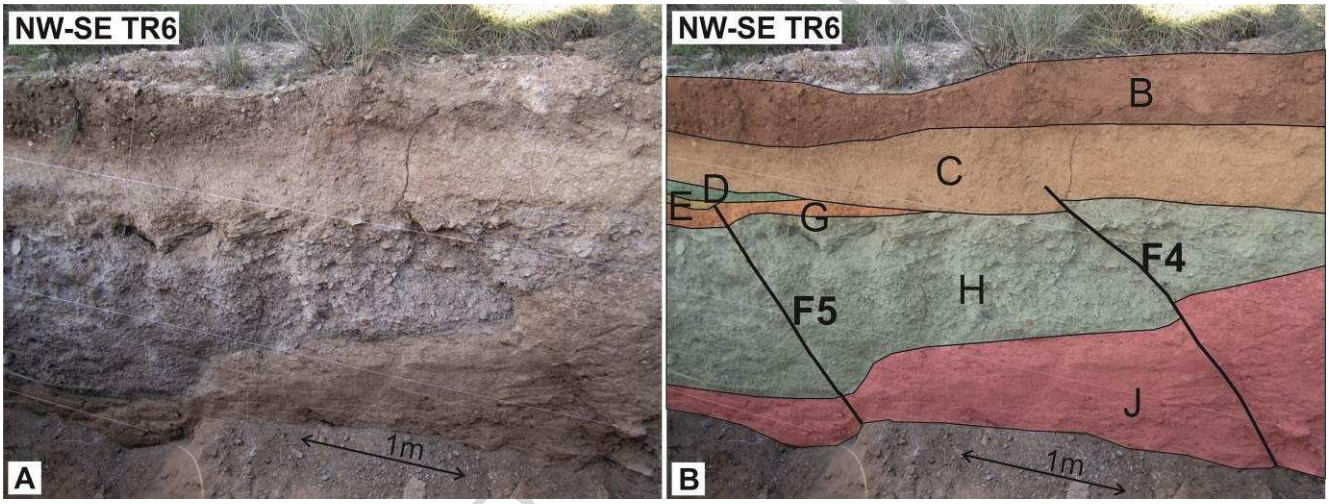

Figure 3. Perspective view of the fault zone in trench 6 (NE wall) and interpretation of the exposed units and fault traces F4 and F5.

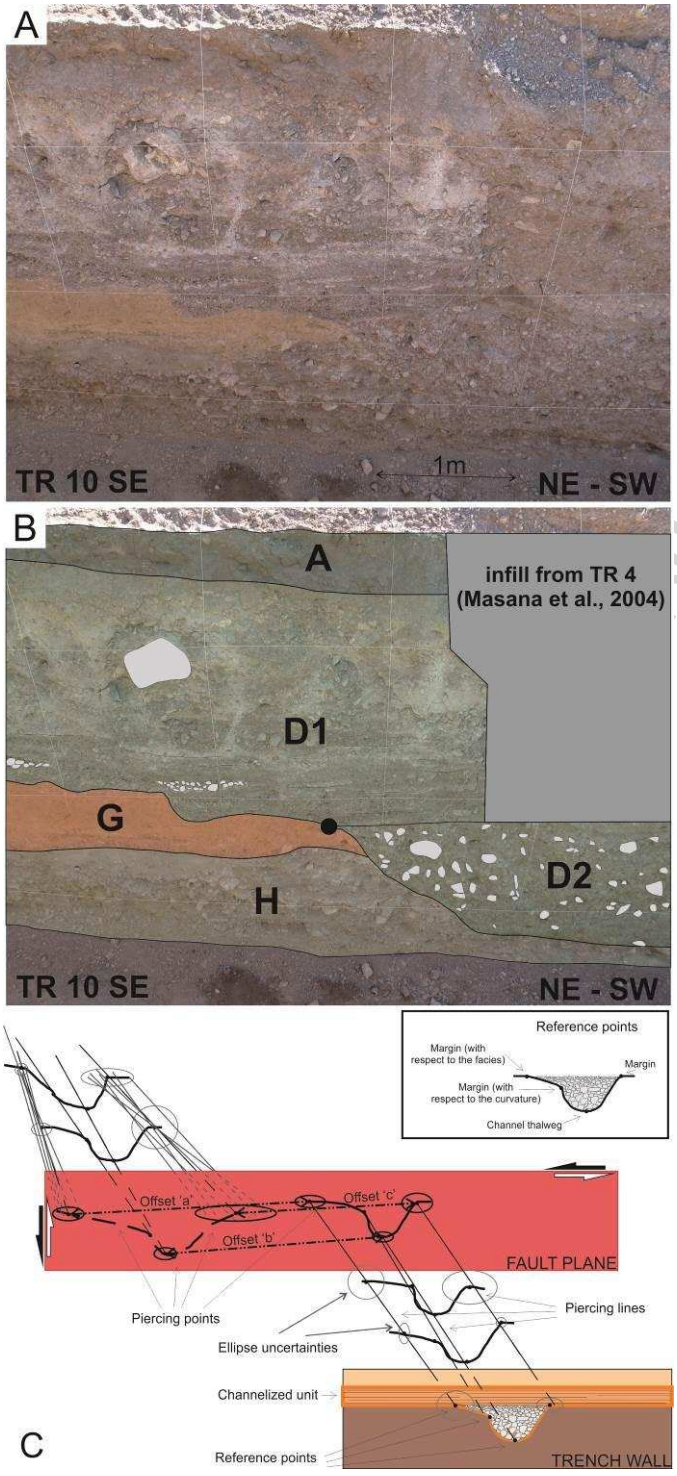

Figure 4. A and B) Field view of unit D. an example of a reference point used to construct the piercing lines (trench 10, SE wall): the infilling of channel D can be divided in two subunits indicating a change in the depositional process: D2 composed of coarse gravels lacking internal organization and D1 composed with finer grained gravels showing better classification and laminar bedding. Unit D2 infills a channelized scar while unit D1 spreads over a wider area. We used the uppermost limit of unit D2 as

an equivalent to the channel bank just before the deposition of unit D1. This same observation was obtained in the rest of the trenches and was used to obtain the piercing lines. An uncertainty on the exact position of each of these reference points was estimated directly in the field. C) Sketch of the channel features used for the analysis, their spatial relationships and the methodological approach to calculate the piercing points. Every channel profile is identified in one trench wall. For two channel features (in the downlifted wall) it is shown how we calculated the piercing point uncertainties on the fault plane based on a Monte-Carlo approach. The uncertainty ellipse around the piercing point was calculated with the intersection of hundreds of random possible piercing lines with the fault plane. The possible random lines are within the uncertainty areas of the reference points. The projection of piercing lines on the fault plane was used to define each piercing point and its associated uncertainty.

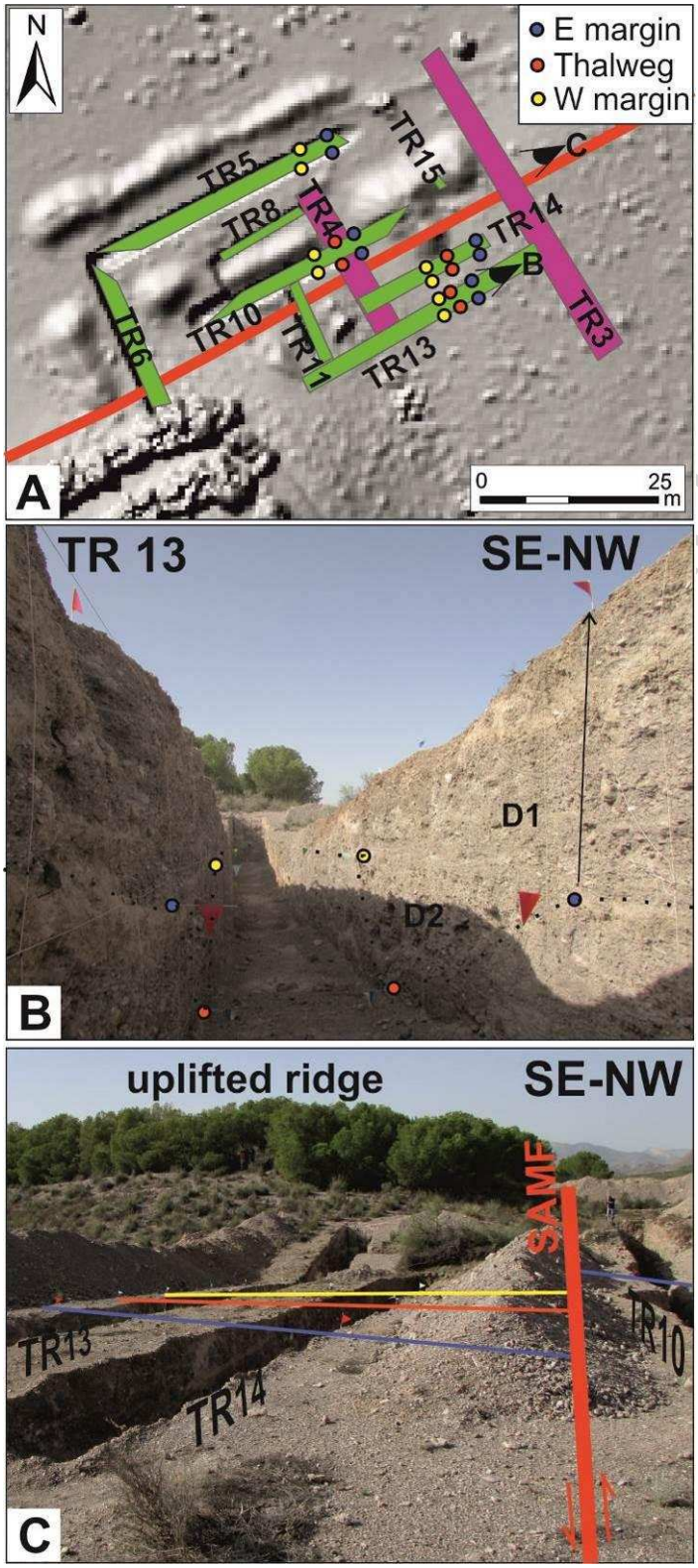

Figure 5. Reference points identified in the trenches. A) Map of the trenches with respect to the surface projection of the reference points identified in the trench walls, the solid red line is the fault zone (the eye symbols indicate the perspectives of the pictures B and D); B) example of the identified reference points of unit D in the trench 13, and their projections on surface; C) field photograph of the trenches

and the projection of the reference points indicated with flags (the approximation of the piercing lines is shown).

HIGHLIGHTS

- 3D trenching yields robust seismic parameters from a slow moving fault
- Reliable slip rate is based on offset buried channels and statistics
- The Alhama de Murcia fault slip rate is much higher than early estimates
- Maximum slip per event value is based on lengthened paleoseismological record
- The Alhama de Murcia fault may be the source of earthquake moment magnitudes > 6.5